15TH IEA HEAT PUMP CONFERENCE
MAY 26–29, 2026 | HOFBURG
VIENNA 2026
DECARBONISATION THROUGH INNOVATION

Design and model-based performance analysis of a low-capacity R-718 high temperature heat pump

Marco Bless[a,*], Davide Tommasini[a], Krzysztof Banasiak[a], Ángel Á. Pardiñas[b]

[a] SINTEF Energy Research, Sem Sælands vei 11, 7034 Trondheim, Norway
[b] ITG Technology Center, 15003 Cantón Grande 9, A Coruña, Spain

Abstract

Available research shows that water, R-718, as a refrigerant can lead to high coefficients of performance, especially at high condensation temperatures above 100°C and high temperature lifts. Using R-718 comes with thermodynamic and operational challenges like the large specific volume at lower pressures, the need for precise superheat control, danger of corrosion and challenge of oil management. To overcome these challenges, R-718 has mainly been used in higher capacity range suitable for turbomachinery. In order to expand the range of applications for R-718 heat pumps towards lower capacities, it is necessary to address these challenges by innovative compressor and system designs.

In this work a Modelica based model was developed as a design-basis for a high temperature heat pump using R-718 as refrigerant. The model consists of a piston compressor with four integrated compression stages, intercooling system and superheat control. To fulfil the requirements of a potential implementation site, the model is tuned to target heat source and sink temperatures of 90±5°C and 180±5°C respectively, corresponding to a temperature lift of 90±5 K. The targeted heating duty is 35 kW. In this paper, the outline and design of the HTHP and the belonging model are presented. Employing the one-dimensional model, a comprehensive performance evaluation is conduced, resulting in a Carnot efficiency of 52%.

Keywords: R-718 ; High temperature heat pump; Piston compressor; Reciprocating compressor; Simulation; Multi-stage

1. Introduction

Decarbonizing industrial heating processes is a critical step toward reducing greenhouse gas emissions and to meet climate targets. Electrification using clean electricity is therefore a key solution, but direct electric heating would significantly increase demand for electricity. Heat pumps offer a more efficient alternative, since electricity is used to upgrade heat from a source instead of generating it. [1]

High-temperature heat pumps (HTHP) are thereby essential for industrial and commercial applications [2]. However, the range of available HTHP remains limited, particularly for temperatures above 150°C [3,4]. The choice of the right working fluid is one of the major challenges. Among natural working fluids, water (R-718) is a promising option due to its unique properties: zero ozone depletion potential (ODP) and zero global warming potential (GWP), as well as being non-toxic, non-flammable, and having low costs [4–7]. Its high latent heat of vaporization and critical temperature of 374°C enable high theoretical coefficient of performance (COP), making it well-suited for high-temperature applications [4,5].

Despite these advantages, R-718 comes with significant technical challenges. At evaporation temperatures below 100°C, operating under vacuum increases the risk of air ingress and component corrosion [5,6]. Its low

* Corresponding author. *E-mail address:* marco.bless@sintef.no

vapour density results in high volumetric flow rates and compression ratios, requiring specialised compressors, such as screw or centrifugal machines [4,7–9]. Other important factors influencing the compressor choice are the superheat control, the material compatibility at high temperatures and, since water and oils are immiscible, the lubrication and sealings [7,8]. Consequently, R-718-based heat pumps have historically been constrained to capacity ranges suitable for turbomachinery and screw compressors [5,10–12].

Recent studies confirm that R-718 achieves superior COP at high condensation temperatures, with performance improving as the condensation temperature increases [7,13]. However, excessive discharge superheat and large compression ratios remain challenges, limiting practical applications [7]. Addressing these challenges requires innovative system architectures and compressor designs, such as multi-stage compression and liquid injection strategies [4,6,7].

In the EU project GeoS-TECHIS [14], an oil-free piston steam compressor for low capacities manufactured by Dorin [15] will be tested to bridge the gap between the temperatures reached with hydrocarbon systems and the already available high-capacity compressors that use steam. The one-dimensional, transient model of this system is presented in this paper. A sensitivity analysis for changing heat sink temperatures will exemplify the strategy for limiting the discharge temperature due to the construction material limitations. Furthermore, the effects on the mass and energy flows, the COP, and the pressures and pressure ratio will be shown.

2. Methodology

The system model, which is described in Section 3, was built in Dymola [16], a comprehensive software platform designed for modelling and simulating complex, integrated systems using the object-oriented programming language Modelica. The TIL Suite library, version 2025.2 [17], which provides validated components and fluid properties for thermal systems, was utilized.

The heat pump unit model was used to enable proper dimensioning of components and for cross-checking of controlling approaches. A sensitivity analysis to the heat sink temperature was carried out to investigate the system behaviour and potential limits in operational envelope, mainly related to the limitation of the discharge temperature.

For this, a quasi-steady state simulation was performed. The quasi-steady state was achieved by using a smooth step function that varied the heat sink inlet temperature from 180°C to 160°C. Using a long duration for this change gave the system time to adjust and reach steady state. Here, the duration was 24 h, leading to a rate of change of roughly 0.83 K/h. An initial comparison between this quasi-steady state method and actual steady state simulations had shown no significant deviation. In direct comparison, using a smooth step function with long duration instead of many steady state simulations enabled a smooth representation of the results, thus avoiding the use of interval reduction techniques at event points.

The heat sink temperature was the only parameter that was changed in the simulation. Other important conditions like the mass flow rate of thermal oil at the condenser and the mass flow rate of water at the evaporator were constant and were set, respectively, to 2.318 kg/s and 3 kg/s. The compressor speed was fixed at 1450 rpm (50 Hz).

For the analysis of the strategy for the limitation of the discharge temperature of the fourth stage, a reference simulation was done, where the feedback valve from the fourth stage discharge to the third stage discharge was kept shut.

2.1. Definition of key performance indicators

The compression ratio (r_c) of each compressor stage i is determined using Eq. (1), where p_dis and p_suc are the discharge and suction pressure, respectively. The overall compression ratio pertains to the suction of first stage and the discharge of the fourth stage.

$$r_{c,i} = p_{dis,i}/p_{suc,i} \tag{1}$$

The coefficient of performance is calculated, as illustrated in Eq. (2), by taking the ratio of the heat flow rate at the condenser ($\dot{Q}_c$) to the overall power consumption of the unit. This power consumption comprises the compressor power (P_{comp}) and the electric heater power, equivalent to its heat flow ($\dot{Q}_{el}$), assuming an efficiency of 1. The electric heater ensures the superheat at the suction of the first stage. The COP of Carnot, denoted as COP_{Ca}, is calculated with Eq. (3), where T_H and T_L correspond to the inlet temperatures of the heat sink and the heat source, respectively, expressed in Kelvin. Lastly, the Carnot efficiency (η_{Ca}) is defined as the ratio of the COP to COP_{Ca}, as shown in Eq. (4).

$$\mathrm{COP} = \dot{Q}_c/\left(P_{comp} + \dot{Q}_{el}\right) \tag{2}$$

$$\mathrm{COP}_{Ca} = T_H/(T_H + T_L) \tag{3}$$

$$\eta_{Ca} = \mathrm{COP}/\mathrm{COP}_{Ca} \tag{4}$$

3. System Design

The heat pump system is designed for R-718 as a refrigerant. The utilized compressor is a four-stage oil-free piston compressor. In addition to the conventional heat pump system with evaporator, compressor, condenser and expansion valve, this system comprises (i) an electric heater for superheating of the first stage suction gas, (ii) interstage desuperheating and (iii) recirculation loop for discharge temperature limitation of the fourth stage. The intercooling combines high-pressure condensate evaporation and liquid injection. The discharge temperature limitation is done by recirculating part of the fourth stage discharge stream to third stage discharge stream. The targeted design parameters for duty and the heat sink and source temperatures are summarized in Table 1. And the overall system model and layout can be seen in Figure 1.

Table 1. General design parameters for the heat pump system.

Design parameter	Target values
Duty	35 kW
Heat source	90±5°C
Heat sink	180±5°C
Pinch approach at heat source	5 K
Pinch approach at heat sink	8 K

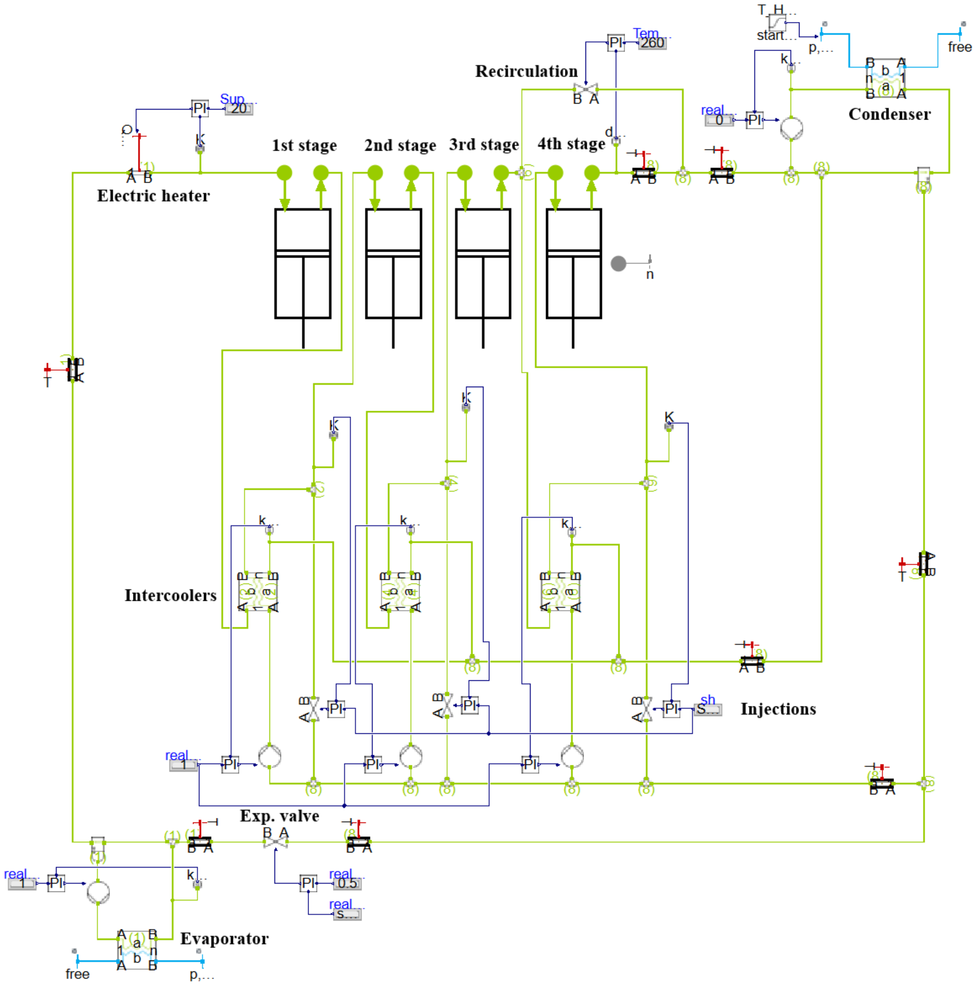

Figure 1. Modelica model of the R-718 heat pump with four compression stages.

3.1. Heat exchangers

The model uses heat exchangers of plate-type. The pressure drop evaluation is neglected in the model. As a heat transfer correlation, a constant heat transfer coefficient is used. The heat exchangers are specified and presented in Table 2. With data from heat exchanger manufacturers on heat transfer area, internal volume, temperatures and duty, the heat transfer coefficients have been adjusted to match the heat exchange performances.

Table 2. Heat exchanger dimensioning parameters.

Heat exchanger	UA[1] [W/K]	Heat transfer area, A [m^2]	Internal Volume (side specific) [dm^3]
Evaporator	4140.80	10.88	8.078
Condenser	2902.16	4.363	4.038
Desuperheater 1	91.32	0.6576	1.44
Desuperheater 2	96.82	0.6576	1.44
Desuperheater 3	104.30	0.6576	1.44

1 [1] UA: product of thermal transmittance (U) and the heat transfer area (A)

In the real system, flooded heat exchangers will be used with separation volumes up-stream to avoid suction or expansion of two-phase fluid. Since modelling of flooded heat exchangers and gravitational loops hits the limitations of the used library, these phenomena are simulated by using a pump that controls the flow over the heat exchangers depending on the vapor or liquid outlet quality. The outlet quality is set to 0, corresponding to saturated liquid, for the condenser, and to 1, corresponding to saturated vapor, for the evaporator and all the intercoolers. The evaporated gas or condensed liquid is then mixed with the fluid prior to the separator inlet. The respective phase of the separator is then cycled over the heat exchanger: the vapor over the condenser and the liquid over the evaporator. The other phase is either superheated and compressed or subcooled and expanded.

Pipes between the main components are used to (i) simulate heat transfer to the ambient and (ii) evaluate their contribution to the overall thermal inertia of the system. The ambient temperature is set to 20°C. As heat transfer model, constant heat transfer coefficients are used again. Those are depending on the expected state in the pipe and are shown in Table 3. The pressure drop is neglected, and the pipes are only scaled to a length of 1 m, limiting the heat transfer.

Table 3. Heat transfer coefficients in pipes

State	Heat transfer coefficient [W/(m^2*K)]
Superheated steam	200
Condensation	10*10^3
Boiling	30*10^3
Forced convection of water	5*10^3

3.2. Compressor model

The compression process consists of four stages of compression with interstage desuperheating. The compressor, which is a reciprocating compressor, was modelled using the standard positive displacement compressor model of the TIL library. The isentropic efficiency (η_{is}) of each compression stage was set to 77.5%, as suggested by the compressor manufacturer. The volumetric efficiency (η_{v}) is calculated with Eq. (5). The relative dead volume (r_{d}) was assumed to be 8%. The heat capacity ratio (k) was assumed to be the mean logarithmic value between its inlet and outlet. The electric motor efficiency was assumed to be 92%.

Finally, the compressor was parametrized with the nominal displacements of each stage listed in Table 4, which were provided by the compressor manufacturer.

$$\eta_{\mathrm{v}} = 1 + r_{\mathrm{d}}/(1 - r_{\mathrm{d}}) * \left(1 - r_{\mathrm{c}}^{1/k}\right) \tag{5}$$

Table 4: Nominal displacements of the four stages of the reciprocating compressor.

Compression stage	Nominal displacement [m^3/h]
1	143.9
2	56.85
3	24.98
4	13.93

3.3. Interstage desuperheating strategy

The desuperheating between the four different compression stages is performed in two steps for every stage. First, in the desuperheating evaporators the high-pressure liquid out of the condenser is evaporated and fed back to the condenser. The desuperheaters are configured as parallel-flow (co-current) heat exchangers. Second, the condensed and subcooled liquid is expanded to the respecting interstage pressure levels and then injected as two-phase fluid to the suction stream of the next higher compression stage.

Like the evaporator, the heat exchangers for the desuperheating are flooded on the evaporation side. The liquid out of the condenser is evaporated at the same pressure level in the desuperheaters of the first, second and third compression stage, where the vapor outlet quality is controlled and kept constant using the feed pumps. The vapor is circulated back to inlet of the separator prior to the condenser. This closes the flooded heat exchanger loop consisting of separating, heat exchange/phase transition and mixing into the feed. Feeding the heat from the interstage desuperheating into the condenser, will boost the heating COP.

3.4. Strategy for the reduction of the discharge temperature

The strategy used for interstage desuperheating focuses on limiting the suction superheat but does not take restrictions on the discharge side into account. Since the manufacturer of the piston compressor limited the maximum allowed discharge temperature to 260°C, an additional solution must be implemented. Since the suction superheat is adjusted already, the only degree of freedom on a system level left to adjust is the pressure. Therefore, partly recycling of the fourth stage discharge to the third stage discharge is used. This increases the suction pressure of the fourth stage and hereby reduces its discharge temperature.

3.5. Control system

Several parameters of the system are actively controlled to achieve stable operation. Table 5 shows an overview of the process variables that are controlled by the associated control variable using proportional and integral control logic. The Skogestad adapted IMC-PID tuning method [18] has been applied to find the best parameters.

Table 5. Process and control variables.

Process variable	Control variable	Set point
Liquid level of the separator of the evaporator	Opening of the expansion valve	0.5
First stage suction superheat	External heat input from el-heater	20 K
Second, third and fourth stage suction superheat	Opening of the valve for desuperheating injection of the associated stage	20 K
Limitation of the fourth stage discharge temperature	Opening of the valve for recirculation from the fourth to third compression stage	260°C
Quality of the flooded heat exchangers' outlets: evaporator, desuperheater 1, desuperheater 2, desuperheater 3, condenser	Mass flow through the heat exchanger, using the respective pump	0 (liquid) or 1 (gaseous)

Since the expansion valve is operated depending on the liquid level of the evaporator's separator and the frequency of the compressor is fixed, the high pressure is floating. It adjusts itself over the liquid-vapor ratio, that is in balance with the heat sink temperature and mass flow, influencing the heat transfer and duty.

3.6. System visualization in the pressure-enthalpy diagram

Figure 2 shows the pressure-enthalpy diagram of R-718 with the state points of the HTHP system. The main cycle is shown in green and has the significant four compression steps, indicated by the points 2 to 3 (first compression stage), 5 to 6 (second compression stage), 8 to 9 (third compression stage), and 11 to 12 (fourth compression stage).

The interstage cooling can be seen as the horizontal lines 3 to 5, 6 to 8 and 9 to 11 respectively for the different stages. The division of the intercooling into the two parts, cooling with high pressure condensate and injection-cooling, is visible. The cooling with high pressure condensate is shown with the points 3 to 4, 6 to 7 and 9 to 10 for the different stages. The injection-cooling lines are coloured differently for easier recognition and comprise of the state points 13-15-5 for the first stage intercooling, of 13-16-8 for the second stage intercooling, and of 13-17-11 for the third stage intercooling.

The recirculation from the fourth stage discharge to the third stage discharge for limiting the fourth stage discharge temperature, is coloured in grey. The fourth stage discharge, point 12, is expanded to the third stage discharge pressure at point 18 and mixes with the third stage discharge from point 9, meeting in point 19.

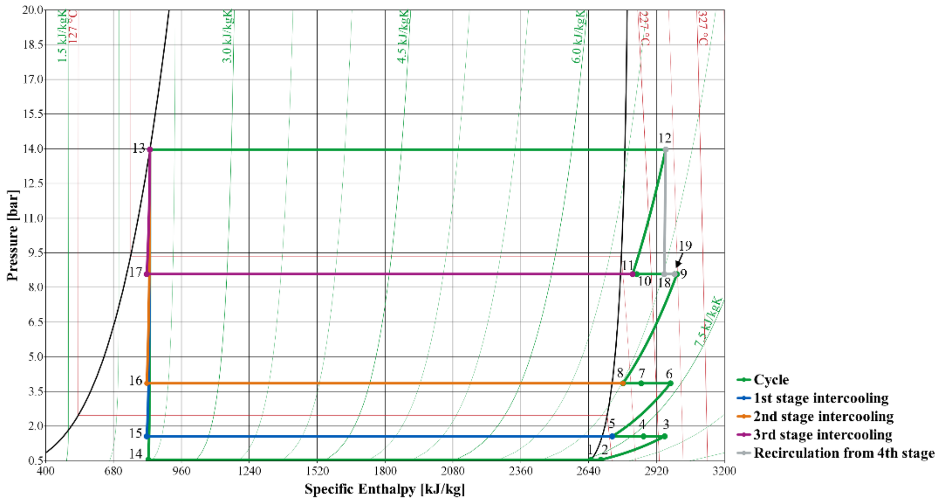

Figure 2. Pressure-enthalpy diagram of the presented R-718 cycle.

4. Simulation results

4.1. Coefficient of performance and energy flows

Figure 3 shows the change in the heating COP with the increasing heat sink inlet temperature for the recirculation of the fourth stage activated and deactivated. The heating COP declines from 3.14 at 160°C heat sink inlet temperature to 2.60 and to 2.66 at 180°C heat sink inlet temperature respectively for the recirculation on and off. The power consumption of the electric heater for the superheating of the first stage suction gas is included in the COP calculations.

The COP loss due to the recirculation on the last stage, needed for technical limitations of the compressor, reaches a penalty of up to 2.5% without deviations due to rounding (2.3% with deviations due to rounding) when the heat sink inlet temperature is 180°C. Due to the steep slope of the curve after the recirculation valve is activated, is evident that the penalty in COP increases with higher heat sink inlet temperatures.

With the heat source inlet temperature of 90°C and the heat sink inlet temperatures between 160°C to 180°C, the ideal temperature lift varies between 70 K to 90 K, leading to Carnot COPs of around 6.2 to 5.04. The Carnot efficiency of the system is therefore in a range of 52±1%.

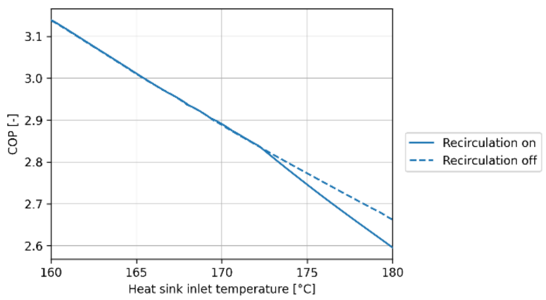

Figure 3. COP at a heat source inlet temperature of 90°C and at various heat sink inlet temperatures both with and without recirculation on the last compression stage.

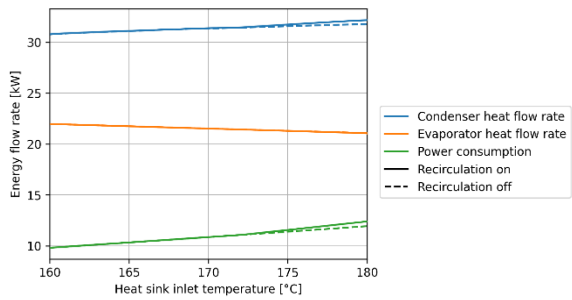

Figure 4. Heat flow rates at the condenser and evaporator, along with power consumption, including both the compressor and electric heater, at a heat source inlet temperature of 90°C and for various heat sink inlet temperatures with and without recirculation on the last compression stage.

Figure 4 presents energy flow rates as heat flow for the evaporator and the condenser and as power for the compressor. Both scenarios with the recirculation on and off are shown. There is no difference between the evaporator heat flow in both scenarios but there is for the condenser heat flow and the power. Both the power and the condenser heat flow increase with the heat sink temperature and at 172.2°C, the increase accelerates for the scenario with the fourth stage recirculation turned on. The evaporator heat flow rate decreases with the heat sink inlet temperature from around 22.0 kW at 160°C to 21.1 kW at 180°C. The heat flow in the condenser increases with increasing heat sink inlet temperature for the case with recirculation activated from 30.8 kW at 160°C to 32.2 kW at 180°C. This additional energy comes from the compressor whose power consumption increases from 9.8 kW to 12.4 kW. Compared to the reference scenario with the recirculation deactivated, the condenser heat increased by 1.3% while the power consumption increased by 3.9% at the highest heat sink inlet temperature.

4.2. Discharge temperature reduction and injection cooling

Figure 5 illustrates the relationship between the outlet temperatures of the different compression stages and the heat sink inlet temperature for the two simulations with the discharge temperature limitation activated and deactivated.

While the compressor discharge temperature for all stages keeps increasing with increasing heat sink inlet temperature, it is evident that from a heat sink inlet temperature of 172.2°C and onwards, the recirculation for limiting the fourth stage discharge temperature to 260°C activates. Without the limiting recirculation, the discharge temperature of the fourth stage rises to approximately 282°C.

Figure 5 also shows that the fourth stage recirculation influences the discharge temperature of the previous stages. While the first and second stage discharge temperatures only show a slight increase at higher heat sink inlet temperatures when the recirculation is activated, the third stage discharge temperature shows a steep increase. At a heat sink inlet temperature of 175.5°C, the third stage discharge temperature even exceeds the limit of 260°C and at 180°C heat sink inlet temperature, the third stage discharge is around 279°C, which is 19 K above the allowed discharge temperature.

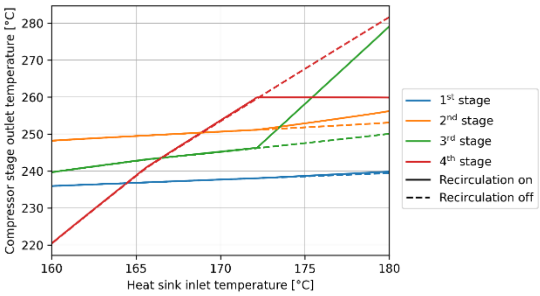

Figure 5. Discharge temperature of the different compression stages with and without recirculation on the last compression stage at a heat source inlet temperature of 90°C.

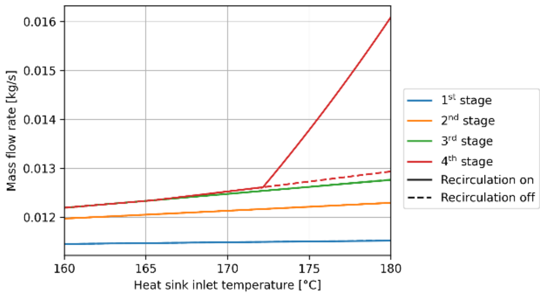

Figure 6. Mass flow rates of the four compression stages with and without recirculation on the last compression stage at a heat source inlet temperature of 90°C.

The plot of Figure 6 shows how the mass flow rate varies with the heat sink inlet temperature across the four compression stages for the simulation and its reference. The initial three stages (blue, orange, green) demonstrate only slight increases as the temperature increases. In contrast, the fourth stage (red) exhibits a sharp increase beyond 172.2°C when the recirculation valve is activated, reaching approximately 0.016 kg/s at 180°C. In the reference simulation, when the valve is kept closed the flow follows the same trend as for the other compression stages. The effect of the injection cooling is visible as the mass flows increase with each stage. The injected flows relative to the previous mass-flow are between 4.5% to 6.7% for the first stage intercooling, between 1.8% to 3.8% for the second stage intercooling and up to 1.0% and 1.3% in the third stage intercooling respectively with and without recirculation. Up to 25.1% of the mass flow rate elaborated by the fourth stage is recirculated to limit its discharge temperature. It is important to note that the injection on the third stage intercooling ceases at heat sink inlet temperatures below 165.4°C. This is due to the superheating at the fourth stage suction being already below the designated setpoint of 20°C, reaching a minimum value of 15.6°C when the heat sink outlet temperature is at 160°C.

4.3. Pressure levels and compression ratios

Figure 7 demonstrates the variation in pressure with respect to heat sink inlet temperature across all compression stages for both scenarios. While the suction and discharge pressure of the first stage remain nearly constant with increases of only 1.0% and 3.6% respectively over the temperature range, the discharge pressure of the second stage rises slightly by 8.2%. At a heat sink inlet temperature of 160°C, the first stage suction and discharge pressure correspond to 0.55 bar and 1.51 bar respectively, while the second stage discharge corresponds to 3.58 bar.

The fourth stage discharge pressure experiences the highest increase of 58% from 8.8 to 14.0 bar at 160°C and 180°C respectively.

Whether or not the recirculation is active influences only the discharge pressure of the third stage significantly. While the pressure rises in the reference scenario with deactivated recirculation nearly linear from 6.4 bar to 7.2 bar, the activated recirculation shows the lift of the third stage discharge pressure that occurs after 172.2°C. From that point, the increase is nearly linear too but with a steeper incline. The pressure increases up to 8.8 bar at 180°C heat sink inlet temperature.

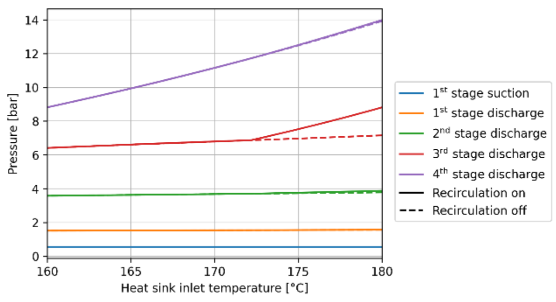

Figure 7. Development of the pressure levels with the heat sink inlet temperature.

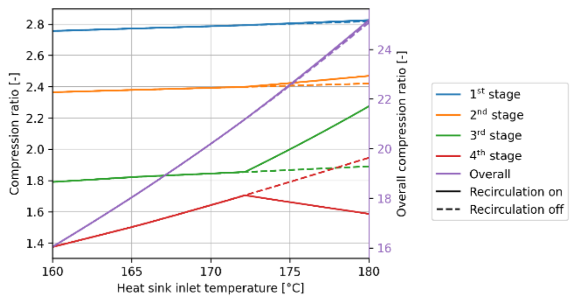

Figure 8. The compression ratios of each stage and the overall compression ratio.

Figure 8 presents the compression ratio for each stage, as well as the overall compression ratio and shows how they change with increasing heat sink inlet temperature. The simulation results for recirculation activated and deactivated, the reference case, are outlined.

While the first compression stage shows the highest compression ratio with values ranging from 2.76 to 2.83, it is – besides the overall compression ratio – the only one that is not significantly influenced by the recirculation. The overall compression ratio is not influenced significantly by the recirculation because the condensing pressure is adjusting depending on the vapor-liquid equilibrium determined by the heat exchange in the condenser. The overall compression ratio ranges from 16.0 at a heat sink inlet temperature of 160°C to 25.2 at 180°C.

It is evident that the pressure ratio is decreasing with a higher compression stage.

5. Discussion

The discharge temperature regulation showed a significant influence on the discharge pressure of the third stage (Figure 7). As intended, this was limiting the discharge temperature of the fourth stage to the targeted 260°C (Figure 5). However, as the recirculation did not lead to a redistribution throughout all compression stages and the influence on the first and second compressor discharge pressures are insignificant, the increase in the third stage discharge pressure increases the pressure ratio of the third stage. Since constant isentropic efficiency is used in the compressor models, the increased pressure ratio leads to higher discharge temperatures. This is also seen in the pressure-enthalpy diagram, Figure 2, as the isentropic lines and the saturated vapor line are growing apart with increasing enthalpy and pressure. However, this results in the third stage discharge temperature exceeding the limit of 260°C at a heat sink inlet temperature of 175.5°C. For heat sink inlet temperatures above that threshold another discharge temperature regulation strategy must be found.

The heating duty initially targeted was 35 kW. The simulation however showed that with the dimensioning of the compressor, only a heating duty of 32.2 kW can be reached, missing the target by 8%. Higher heating duties could be reached by adjusting the nominal displacement (Table 4). But the nominal displacement was calculated based on the compressor design of the manufacturer. Since other limitations like the cylinder bore play a vital role in manufacturing processes, meeting an exact heating duty target is challenging.

A Carnot efficiency of 52±1% was identified. With HTHP systems usually being in a range of 40 to 60%, the simulation results showed good system performance, yet leaving room for improvement. However, the performance of a real system can be expected to be lower as the model does not take losses due to pressure drop into account, nor is the heat loss to the ambient sized correctly yet. The isentropic compressor efficiency is also constant. The performance prognosis should therefore be viewed as a benchmark.

6. Conclusion

This study successfully addressed several key challenges associated with using R-718. The issue of large compression ratios was effectively mitigated by implementing four compression stages, while desuperheating was managed through cooling with high pressure condensate and liquid injection.

The sensitivity analysis of the heat sink temperature provided important insights into the system behaviour. The strategy to limit the fourth stage discharge temperature to 260°C proved effective up to a heat sink inlet temperature of 172.2°C, where the recirculation from the fourth stage discharge to the third stage discharge was activated. However, a side effect was observed: the elevated third-stage discharge pressure influenced its discharge temperature, which exceeded the 260°C limit at a heat sink inlet temperature of 175.5°C. Beyond this point, a new discharge temperature regulation strategy will be required.

The performance evaluation demonstrated that the heat pump system achieved high COPs, ranging from 3.14 at 160°C heat sink inlet temperature to 2.60 at 180°C, with a heat source temperature of 90°C. Although a performance penalty of up to 2.5 % was identified due to the discharge temperature limitation, the system maintained a Carnot efficiency of 52 ± 1 %, confirming its competitiveness compared to alternative system designs.

Future work will focus on refining the discharge temperature limitation strategy and improving the model with respect to pressure drop and pipe sizing, ensuring further optimization of system performance and reliability.

Acknowledgements

This work has been carried out as a part of the EU project GeoS-TECHIS, Grant Agreement Nr 101172928. The authors gratefully acknowledge the support from the partners of GeoS-TECHIS, the European Union and the compressor manufacturer Dorin for data input and supporting discussions.

Disclaimer

Artificial Intelligence tools were used to assist in language refinement and clarity during the preparation of this manuscript. All technical content, data analysis, and conclusions were developed and validated by the authors.

References

[1] DNV. Global Energy Transition Outlook 2025. DNV 2025. https://www.dnv.com/energy-transition-outlook/2025/ (accessed November 17, 2025).
[2] de Boer R, Marina A, Zühlsdorf B, Arpagaus C, Bantle M, Wilk V, et al. Strengthening Industrial Heat Pump Innovation - Decarbonizing Industrial Heat 2020.
[3] International Energy Agency - Heat Pump Technologies. ANNEX 58 about HTHP Task 1: Technologies – State of the art and ongoing developments for systems and components. Annex 58 n.d. https://heatpumpingtechnologies.org/annex58/task1/ (accessed March 5, 2024).
[4] Wang R, Yan H, Wu D, Jiang J, Dong Y. High temperature heat pumps for industrial heating processes using water as refrigerant. Energy 2024;313:133847. https://doi.org/10.1016/j.energy.2024.133847.
[5] Wu D, Hu B, Wang RZ. Vapor compression heat pumps with pure Low-GWP refrigerants. Renew Sustain Energy Rev 2021;138:110571. https://doi.org/10.1016/j.rser.2020.110571.
[6] Hu B, Wu D, Liang J, Wang RZ. Natural refrigerants in heat pump systems. 2020. https://doi.org/10.18462/IIR.GL.2020.1010.
[7] Shi X, Zhang C, Liu Y, Wang F. Investigation on multi-stage compression high-temperature heat pump system based on R718 and other low GWP refrigerants. Int J Refrig 2025;176:238–53. https://doi.org/10.1016/j.ijrefrig.2025.04.019.
[8] Hanslik F, Suess J, Koehler J. The potential of water as a refrigerant - past, present and future approaches. 2019. https://doi.org/10.18462/IIR.ICR.2019.0474.
[9] International Energy Agency. ANNEX 58 on High-Temperature Heat Pumps Task 1 report: Technologies – State of the art and ongoing developments for systems and components. Annex 58 n.d. https://heatpumpingtechnologies.org/annex58/task1/ (accessed March 25, 2024).
[10] Kharazi AA, Müller N. Comparing Water (R718) to Other Refrigerants, American Society of Mechanical Engineers Digital Collection; 2007, p. 85–93. https://doi.org/10.1115/IMECE2006-13341.
[11] Hanslik F, Suess J, Hanslik F, Suess J. Water as a Refrigerant in Centrifugal Compressor Cooling Systems for Industrial Applications. Adv. Cool. Technol. Appl., IntechOpen; 2018. https://doi.org/10.5772/intechopen.79614.

[12] Zühlsdorf B, Poulsen JL, Dusek S, Wilk V, Krämer J, Rieberer R, et al. ANNEX 58 High-Temperature Heat Pumps - Task 1: Technologies – State of the art and ongoing developments for systems and components 2023.

[13] Wu D, Hu B, Wang RZ, Fan H, Wang R. The performance comparison of high temperature heat pump among R718 and other refrigerants. Renew Energy 2020;154:715–22. https://doi.org/10.1016/j.renene.2020.03.034.

[14] GEOS-TECHIS - Efficient Industrial geothermal processes 2024. https://geos-techis.eu/ (accessed November 3, 2025).

[15] Dorin S.p.A. DORIN innovation n.d. https://www.dorin.com/ (accessed November 15, 2025).

[16] Dymola. Dassault Systèmes 2023. https://www.3ds.com/products/catia/dymola (accessed November 10, 2025).

[17] TLK-Thermo GmbH. TIL Suite 2052.2 [software] 2025. https://www.tlk-thermo.com/en/software/til-suite (accessed November 10, 2025).

[18] Skogestad S. Simple analytic rules for model reduction and PID controller tuning. J Process Control 2003;13:291–309. https://doi.org/10.1016/S0959-1524(02)00062-8.